journal

J. Am. Ceram. Soc., 93 [3] 709–715 (2010)
DOI: 10.1111/j.1551-2916.2009.03498.x

Pressureless Sintering t-zirconia@δ-Al_2O_3 (54 mol%) Core–Shell Nanopowders at 1120°C Provides Dense t-Zirconia-Toughened α-Al_2O_3 Nanocomposites

Min Kim and Richard M. Laine[†,**]

Department of Materials Science and Engineering, University of Michigan, Ann Arbor, Michigan 48109-2136

Zirconia-toughened alumina (ZTA) is of growing importance in a wide variety of fields exemplified by ZTA prosthetic implants. Unfortunately, ZTA composites are generally difficult to process because of the need to preserve the tetragonal zirconia phase in the final dense ceramic, coincident with the need to fully densify the α-Al_2O_3 component. We report here that liquid-feed flame spray pyrolysis of mixtures of metalloorganic precursors of alumina and zirconia at varying compositional ratios provide access in one step to core–shell nanoparticles, wherein the shell is δ-Al_2O_3 and the core is a perfect single crystal of tetragonal (*t*-) zirconia. Pressureless sintering studies provided parameters whereby these nanopowder compacts could be sintered to full density (>99%) at temperatures just above 1100°C converting the shell component to α-Al_2O_3 but preserving the *t*-ZrO_2 without the need for any dopants. The final average grain sizes of these sintered compacts are ≤200 nm. The resulting materials exhibit the expected response to mechanical deformation with the subsequent production of monoclinic ZrO_2. These materials appear to offer a low-temperature, low-cost route to fine-grained ZTA with varied Al_2O_3:*t*-ZrO_2 compositions.

I. Introduction

Partially stabilized tetragonal zirconia (PSZ) has received exceptional attention because it is a part of a special class of ceramics noted for their high toughness.[1–10] This toughness extends from grains responding to applied stress with a tetragonal to monoclinic phase transformation coincident with a 4.0 vol% increase creating stress fields around the transformed grain, greatly limiting crack propagation, and thereby toughening the ceramic.

Multiple additives are used to partially stabilize the tetragonal phase during processing. Yttria is the most common additive with 3 wt% typical for average grain sizes (AGSs) ≥ 1 μm (3YPSZ, 1.6 unit mol%).[11–17] The literature suggests that less yttria is required to partially stabilize finer grained ceramics.[17,18] For example, only 1.5 wt% is needed to stabilize materials with AGSs ≤ 160 nm.

3YPSZ materials are used for applications ranging from multiple types of prosthetic implants, to ceramic knives, thin-film electronic devices, photonic band gap devices, to auto exhaust catalysts.[1–17] Unfortunately, 3YPSZ undergoes unwanted phase transformation to the monoclinic phase in humid environments even at ambient conditions.[18–21] This problem is resolved by forming composites with harder, higher tensile strength and more weather-resistant materials e.g. α-Al_2O_3. Thus, 3YPSZ-toughened α-Al_2O_3 or zirconia-toughened alumina (ZTA) composites are currently considered the next-generation material for prosthetic applications as well as for many applications where 3YPSZs have been used.[18–28]

ZTA composites offer toughening proportional to their 3YPSZ content.[18–42] Unfortunately, the very properties that render the α-Al_2O_3 component valuable also renders it difficult to densify ZTA composites, e.g. α-Al_2O_3 has quite low self-diffusion rates.[42] Typical ZTAs contain ≤30 wt% (26 mol%) 3YPSZ. Compositions ≥ 30 wt% become increasingly more difficult to densify due to these low diffusion rates.[39,40] While hot isostatic pressing (HIPping) can overcome these problems, even HIPped ZTA densities are often <99%.[34–36]

Here, we report the use of $(t\text{-}ZrO_2)_x(\delta\text{-}Al_2O_3)_{1-x}$ core–shell nanopowders produced by liquid-feed flame spray pyrolysis (LF-FSP)[43–48] with average particle sizes (APSs) of 30–50 nm (Fig. 1) to produce fully dense, ultrafine ZTA composites with densities ≥ 99 at 54 unit mol% *t*-ZrO_2 and with final grain sizes <200 nm by pressureless sintering in air at 1120°C. During densification, the *t*-ZrO_2 is retained whereas the original δ-Al_2O_3 shell phase transforms to the α-Al_2O_3 phase below the normal phase transformation temperatures (≈1200°C). Furthermore, simple stress tests by hand grinding demonstrate phase transformation to the monoclinic phase demonstrating that these ZTA materials offer toughening at zirconia loadings heretofore impossible to process.

It appears that *t*-ZrO_2@δ-Al_2O_3 materials exhibit a novel densification mechanism that allows facile processing of these very important commercial materials requiring much less energy, equipment, and time-demanding conditions than ever before possible. Furthermore, it is now possible to greatly increase the *t*-ZrO_2 phase content implying the potential for much greater toughness in these new ZTA ceramics. Both observations suggest that *t*-ZrO_2@δ-Al_2O_3 materials could greatly expand the utility of ZTA ceramics.

II. Experimental Procedure

(1) LF-FSP Processing of Powders

Ethanol solutions were prepared containing mixtures of the precursors alumatrane, $N(CH_2CH_2O)_3Al$, and $Zr(OH)_2(O_2CCH_2CH_3)_2$ at 1–3 wt% Al_2O_3 and ZrO_2 in specific ratios to produce $(t\text{-}ZrO_2)_x(\delta\text{-}Al_2O_3)_{1-x}$ where $x = 0.1$, 0.3, 0.5, or 0.9. These solutions were then aerosolized with oxygen at rates of 50–100 mL/min into a 1.5 m × 30 cm diameter quartz tube and ignited with methane pilot torches creating turbulent flames wherein combustion temperatures reached >1500°C at a point approximately 20 cm along the tube. The combustion products including the ceramic oxide nanopowder "soot" are quenched with atmospheric makeup air such that temperatures drop to 300°–400°C at the end of the tube. The powders are captured in aluminum wire-in-tube electrostatic precipitators maintained at 10 kV DC charge.

Dynamic light scattering (*DLS*) was also used to estimate APSs of LF-FSP nanopowders. Suspensions of each nanopowder in DI water (~1 vol%) were loaded in a compact

V. Jayaram—contributing editor

Manuscript No. 26168. Received April 16, 2009; approved October 21, 2009.
This work was supported by the Air Force Office of Scientific Research, through contracts No. F49620-03-1-0389 and subcontract from UES Inc. F074-009-0041/AF07-T009.
**Fellow, The American Ceramic Society.
[†]Author to whom correspondence should be addressed. e-mail: talsdad@umich.edu

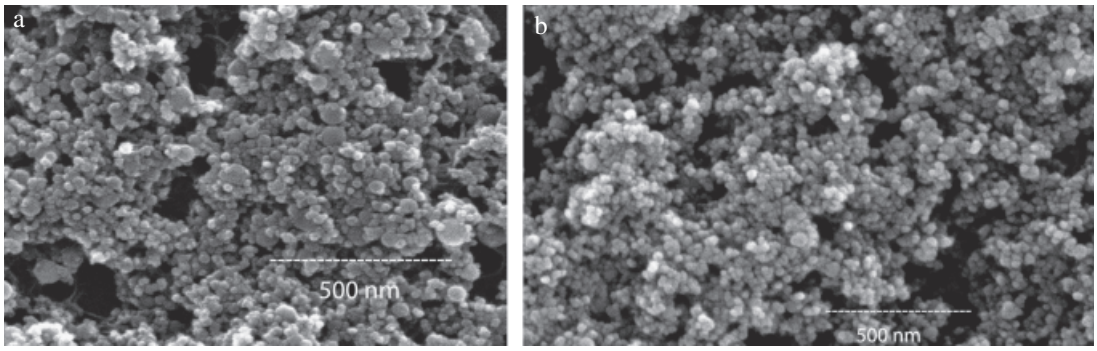

Fig. 1. Scanning electron microscopic images of (a) $(t\text{-}ZrO_2)_{0.13}(Al_2O_3)_{0.87}$ and (b) $(t\text{-}ZrO_2)_{0.54}(Al_2O_3)_{0.46}$ nanopowders.

goniometer system (ALV, Langen, Germany) equipped with a multi-tau digital correlator (ALV-5000E, Langen). The laser source had a wavelength of $\lambda_0 = 0.488$ μm (Innova 70C, Coherent Inc., Santa Clara, CA).

X-ray diffraction (*XRD*) *analyses* were performed on a Rigaku Miniflex (Rigaku, The Woodlands, TX). The diffractometer is equipped with a Cu X-ray tube (Cu$K\alpha$1, l = 1.54059 Å) with operating voltage of 30 kV and current of 15 mA. Scans were performed continuously from 20° to 80° 2θ in 0.03° increments at 2°/min. The nanopowder samples were prepared by packing ~100 mg into an amorphous silica holder and loaded into the diffractometer. Scan data were analyzed using Jade 7.5 software (Materials Data Inc., Livermore, CA) to determine APSs and phases present.

Scanning electron microscopy (SEM) micrographs were taken using a Nova 600 Nanolab FIB/SEM (FEI Company, Hillsboro, OR). About 1 mg of the nanopowder sample was first dispersed in 5 mL of DI water using an ultrasonic horn (Vibracell, Sonics and Materials Inc., Newton, CT) for 10 min. A drop of the dispersion was placed on a SEM sample stub, which was heated on a covered hot plate and the water was allowed to evaporate. The stubs were then sputter-coated with ~180 Å of Au–Pd using a Technics Hummer VI sputtering system (Anatech, Ltd., Alexandria, VA) to improve resolution.

(2) Transmission Electron Microscopy (TEM)

An analytical high-resolution TEM (Model 3011, JEOL, Osaka, Japan) was used to measure the particle sizes and morphologies of as-prepared powders. Powder samples were prepared by dipping a holey carbon grid in a vial of emulsion with as-prepared powder. The specimen was held in a Gatan double tilt goniometer. An operating voltage of 300 kV was used.

(3) Fabrication of green bodies

As-produced LF-FSP powders (3.0 g) were dispersed with 5 mg DARVAN C-N (R.T. Vanderbilt Company Inc., Norwalk, CT) in 100 mL EtOH using a 500 W ultrasonic horn for 12 h followed by sedimentation for 24 h. Then, 5 mg of PEG 3400 D was added and ultrasonification continued for an additional 6 h. The solvent was removed and the recovered powders were vacuum-dried (12 h/200°C), ground lightly (30 min), and sieved through a −325 nylon mesh. This powder (600 mg) was pressed (50 MPa) using a dual-action 12.5 mm WC die, then cold isostatically pressed at 200 MPa/6 h. The binder was removed by heating to 800°C (1°C/min/air/6 h dwell). The resulting pellets were then weighed and their densities were analyzed using both geometrical mean and Archimedes methods.

(4) Theoretical Density Calculations

The theoretical density values where computed using the known values of the end members [δ-Al_2O_3 (3.6 g/cm^3), α-Al_2O_4 (3.99 g/cm^3), and t-ZrO_2 (6.05 g/cm^3)], the composition of the core–shell materials produced, and interpolating using compositions in mol% for the various samples.

(5) Dilatometry Studies

Dilatometry was run using a Theta Industries Dilatronic 6500 (Port Washington, NY) with a thermal expansion head under mild compression. Data were collected from using LabView program. Flat, square pellets, average 1.27 mm on a side, used for the dilatometry runs were sectioned from 12.5 mm disks made as above and placed between an alumina block and the alumina push rod. Constant heating rate (CHR) experiments were conducted with a heating rate of 5°C/min to 1450°C in static air/oxygen.

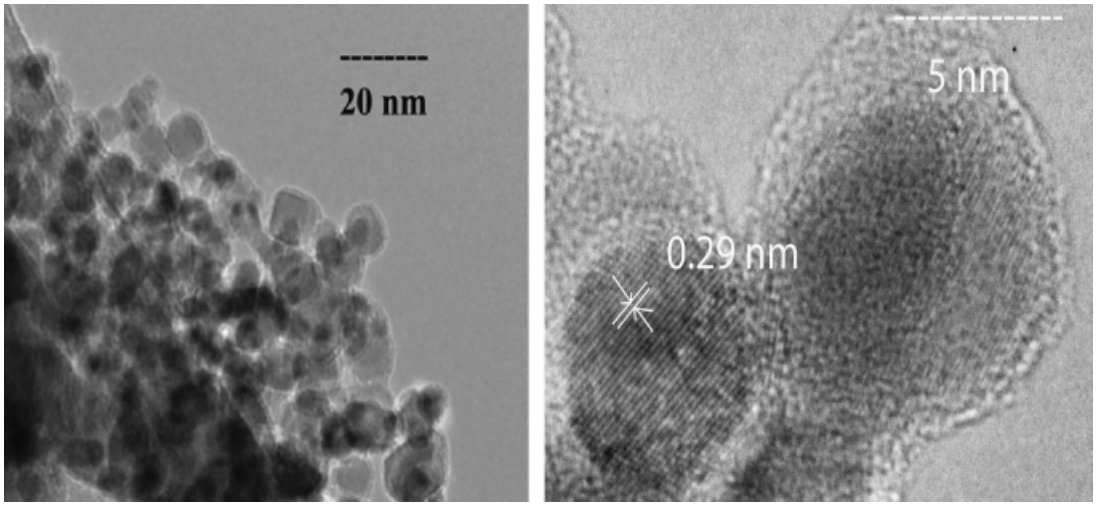

Fig. 2. Transmission electron microscopic images of $(t\text{-}ZrO_2)_{0.54}(Al_2O_3)_{0.46}$ nanopowders.[48]

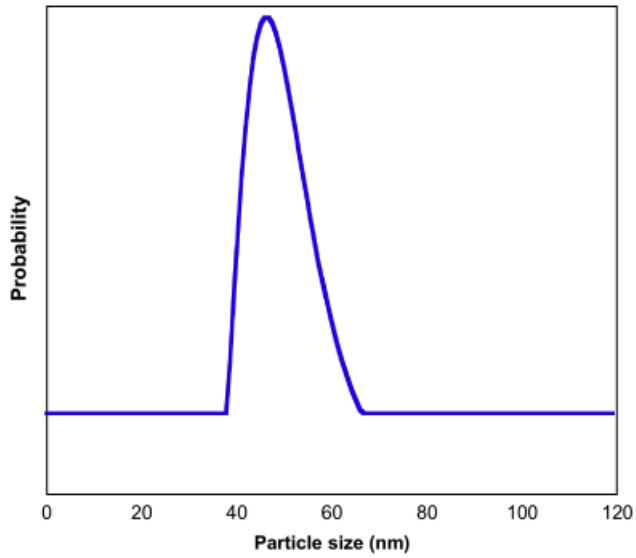

Fig. 3. Dynamic light scattering data of $(t\text{-}ZrO_2)_{0.54}(Al_2O_3)_{0.46}$ nanopowders (average of 20 runs).

(6) Grinding Ceramic Composites

The $(t\text{-}ZrO_2)_{0.54}(\alpha\text{-}Al_2O_3)_{0.45}$ sample sintered at 1120°C was used in an attempt to observe the tetragonal-to-monoclinic zirconia phase transformation, as the evidence of partially stabilized zirconia. A portion of sintered $(ZrO_2)_x(Al_2O_3)_{1-x}$ pellet was cut with a diamond saw to a flat, square pellet, 0.5 mm on a side and ground in an alumina mortar with an alumina pestle, and XRD patterns of ground powders were recorded at the time of the fracture and after 1, 5, and 10 min of grinding.

III. Results and Discussion

We begin by describing the synthesis and general characteristics of our source materials. Thereafter, we discuss compact preparation and sintering conditions.

We have previously described the use of LF-FSP to synthesize a wide variety of nanopowders.[43–48] In the current studies, mixtures of the zirconium carboxylate, $Zr(OH)_2(O_2CCH_2CH_3)_2$, and alumatrane $[Al(OCH_2CH_2)_3N]$ were dissolved in appropriate ratios in ethanol (see "Section I") at 1–3 wt% loading (as ceramic) and aerosolized with oxygen into a quartz combustion chamber. The aerosol was ignited using methane/O_2 pilot torches causing combustion temperatures $\geq$1500°C. External air was used to quench the combustion products $\approx$1.5 m along the chamber such that temperatures fall to 300°–400°C resulting in unaggregated nanoparticles of essentially the same composition as in the precursor solution.

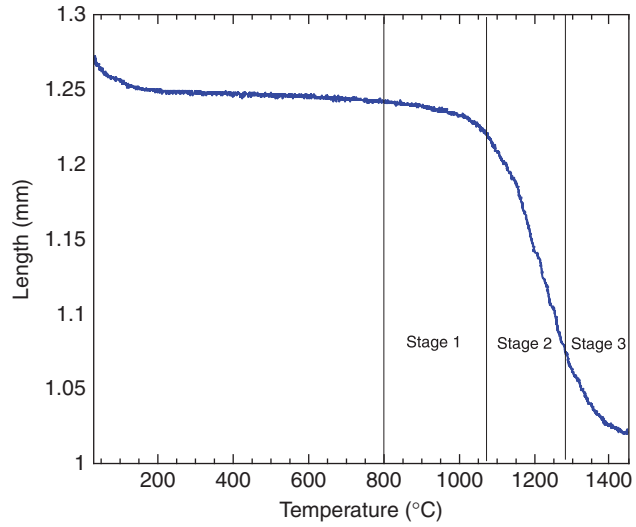

Fig. 4. Dilatometry plot of $(ZrO_2)_{0.54}(Al_2O_3)_{0.45}$ compact ramped at 5°C/min/air to 1425°C/no dwell (average of six different runs).

Table I. Relative Densities of $(ZrO_2)_{0.54}(Al_2O_3)_{0.46}$ Pellet Versus Final Dwell Temperatures

Processing conditions	Relative density†
Before binder burn-out	0.46
After binder burn-out	0.51
Heat to 1070°C (10°C/min/air)	0.83
Heat to 1120°C (10°C/min/air)	0.99
Heat to 1125°C (10°C/min/air)	0.99
Heat to 1145°C (10°C/min/air)	0.99
Heat to 1200°C (10°C/min/air)	0.99

†Density measurements were carried out using the Archimedes method. Average of three measurements.

Figures 1–3 provide SEMs, TEMs, and dynamic laser light scattering (DLS) of $t\text{-}ZrO_2$@δ-Al_2O_3 core–shell powders.[48] The SEMs are presented simply to demonstrate that over the range of powders produced, the particle sizes are very similar and there are no micrometer-sized outliers. The TEM *d*-spacings confirm the XRD results showing a *t*-zirconia core in a δ-Al_2O_3 shell. The DLS data are provided to demonstrate that the LF-FSP process provides powders free from aggregates, which would be expected to present at least a bimodal size distribution.

One of the first papers on pressureless sintering of nanopowders was published by Rhodes in 1981.[49] In this work, Rhodes describes the essentially complete densification (99.5%) of nano (12 nm APS) 6YPSZ at 1100°C with final AGSs of 200 nm. In complementary work,[50] we recently prepared nano-α-Al_2O_3 with APSs of 30–40 nm and were able to pressurelessly sinter them to 99.5% density with final AGSs of 400 nm but only on heating to temperatures >1350°C. Given that the $(t\text{-}ZrO_2)_{0.54}(Al_2O_3)_{0.46}$ shell is δ-Al_2O_3, a defect spinel, these materials might be expected to sinter to full density at much lower temperatures than nano-α-Al_2O_3 and certainly without HIPping, as is a common practice for most ZTAs.

(1) Sintering studies

The sintering behavior of debindered 800°C pellets (see "Section I") was first assessed via dilatometry as shown in Figure 4, which indicates that densification begins just above 1000°C. Note that binder burnout was performed at 800°C to be consistent with previous studies.[51] Significant densification occurs in

Table II. Density Data of Each Sample

Processing conditions	Phase	Theoretical density (g/cm³)*	Measured density (g/cm³)
Before binder burn-out	*t*-zirconia, δ-alumina	5.02	2.30±0.01
After binder burn-out	*t*-zirconia, δ-alumina	5.02	2.56±0.01
Heat to 1070°C (10°C/min/air)	*t*-zirconia, δ-alumina	5.02	4.16±0.01
Heat to 1120°C (10°C/min/air)	*t*-zirconia, α-alumina	5.14	5.09±0.01
Heat to 1125°C (10°C/min/air)	*t*-zirconia, α-alumina	5.14	5.09±0.01
Heat to 1145°C (10°C/min/air)	*t*-zirconia, α-alumina	5.14	5.11±0.01
Heat to 1200°C (10°C/min/air)	*t*-zirconia, α-alumina	5.14	5.11±0.01

*Theoretical density of: *t*-zirconia = 6.05 g/cm³; δ-alumina = 3.60 g/cm³; α-alumina = 3.99 g/cm³. It is important to recognize that in nanosized powders and in nanostructured materials because of the significant volume fraction of grain boundaries, the use of theoretical densities can only approximate the true densities of these composite materials.

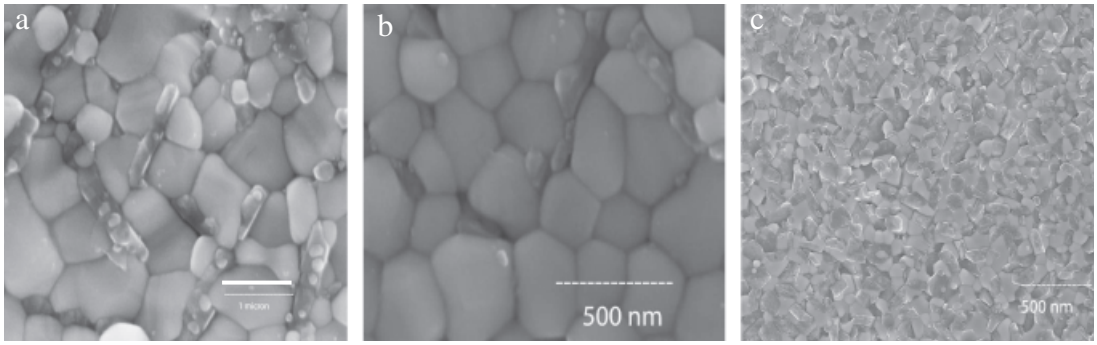

Fig. 5. As-produced surfaces of $(ZrO_2)_{0.54}(Al_2O_3)_{0.46}$ pellets heated to; (a) 5°C/min/air to 1425°C/no dwell (scale bar 1 μm); (b) 10°C/min/air to 1200°C/6 h dwell, and (c) 10°C/min/air to 1120°C/6 h dwell.

the section labeled Stage 2 as witnessed by the very steep slope associated with a high rate of shrinkage at ≈1100°C. These results suggest that our initial concept that the δ-Al_2O_3 shell would sinter first was correct. Based on these studies, we selected ramp rates of 10°C/min/air, final dwell temperatures and times of 1050°–1200°C, and 6 h. Tables I and II results suggest that full density is achieved at ≥1120°C, as might be expected from the Fig. 4 data.

(2) Microstructures of Composites

Figure 5 shows the original surfaces of pellets sintered at selected temperatures including the Fig. 4 dilatometer sample as Fig. 5(a). This sample appears dense with AGSs ≥ 1 μm indicating excessive grain growth in the Fig. 4 stage 3 region, above 1300°C. At 1200°C, Figs. 5(b) and 6(a) (polished surface) show AGSs for the surface and substructure of only 500 nm at full density. At 1120°C, Figs. 5(c) and 6(b) show AGSs of 200 nm and a fully dense microstructure after polishing using diamond media.

At 1070°C, Fig. 6c, the final composite is not fully dense, matching Table I density data (0.83). Figure 4 suggests that it might be possible to completely densify samples at this temperature but with longer dwell times or by HIPping, which could lead to still finer microstructures. In contrast, Fig. 7 shows an HR-SEM of the final microstructure of a pellet made from a 50:50 (mol:mol) *t*-ZrO_2 and δ-Al_2O_3 nanopowders using the same experimental procedure as discussed below. As can be seen, very little if any densification is observed under sintering conditions essentially identical to the $(ZrO_2)_{0.54}(Al_2O_3)_{0.46}$ pellets of Fig. 5. This further supports our contention that the core shell system offers unexpected benefits not anticipated from the literature nor even using our own powders separately. These results receive additional support from the Fig. 8 XRD data.

The Fig. 8 data indicate that the *t*-ZrO_2 transforms to *m*-ZrO_2 at temperatures >1120°C. However, Table I, Figs. 6(c),and 5(c) all demonstrate that at 1120°C, the fully dense composites that retain the *t*-ZrO_2 phase are obtained. One observation that deserves comment is the fact that sintering to 1125°C rather than 1120°C leads to significant transformation to *m*-ZrO_2. Because the dwell time at temperature is 6 h, one might suggest that nucleation of the tetragonal-to-monoclinic transformation is difficult at this temperature but once some nucleation occurs, it can act to seed the transformation process. This would explain the seemingly rather abrupt nature of the behavior observed as a consequence of an approximate 5°C change in processing temperature. It is also important to note that the dilatometry studies clearly indicate a very steep change in densification rates at these temperatures, which also likely contributes to the observed results.

Because of the very large relative index of reflectance (RIR) differences between ZrO_2 and Al_2O_3 in the XRD, we resorted to spot-by-spot XRD analyses in specific 2θ° regions to identify the Al_2O_3 phase in the 1120°C sample (Fig. 9). By comparing the (012), (113), and (116) peaks with those of an α-Al_2O_3 standard (PDF 71-1124), we find that α-Al_2O_3 is the primary phase in the 1120°C nanocomposites.

As discussed in part above, for comparative purposes we prepared identical compacts from mixtures of LF-FSP produced *t*-ZrO_2 and δ-Al_2O_3 using identical procedures (Fig. 7). At 1120°C, we observe final densities of 0.89 ± 0.02 and 100% conversion (by XRD) to *m*-ZrO_2. One conclusion is that the shell preserves the tetragonal phase during processing, perhaps by acting as a compressive coating.

(3) Phase Transformation Toughening

Given that we observe a high proportion of *t*-ZrO_2 in our 1120°C composites, we assessed the potential for transformation toughening via hand grinding. Samples were hand ground using an Al_2O_3 mortar and pestle for 1, 5, and 10 min. As per Fig. 10, the amount of *m*-ZrO_2 increases with increases in grinding time. After 10 min of grinding, the wt % of monoclinic phase is close to 50%.

As noted above, most reported ZTA composites contain a maximum of 30 wt% (26 mol%, 24 vol%) YPSZ with final

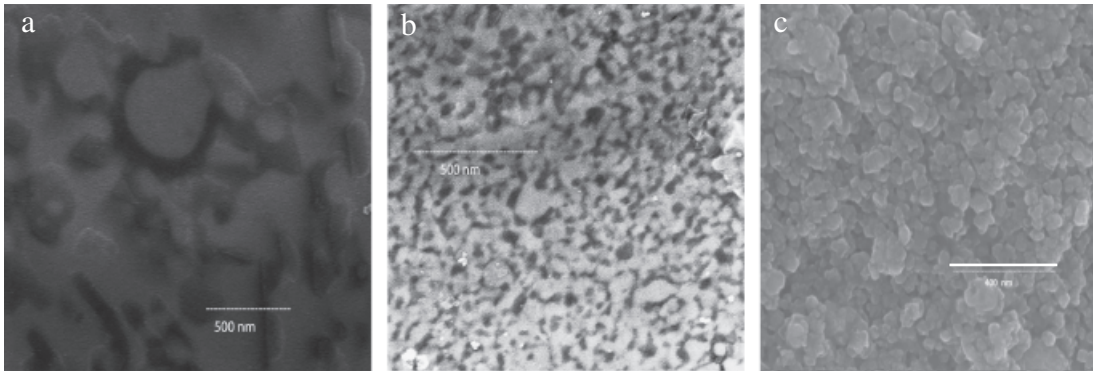

Fig. 6. High-resolution scanning electron microscopy of $(ZrO_2)_{0.54}(Al_2O_3)_{0.46}$ pellets heated to; (a) 10°C/min/air to 1200°C/6 h dwell, polished surface, (b) 10°C/min/air to 1120°C/6 h dwell, polished surface, and (c) 10°C/min/air to 1070°C/6 h dwell (unpolished), (scale bar 400 nm).

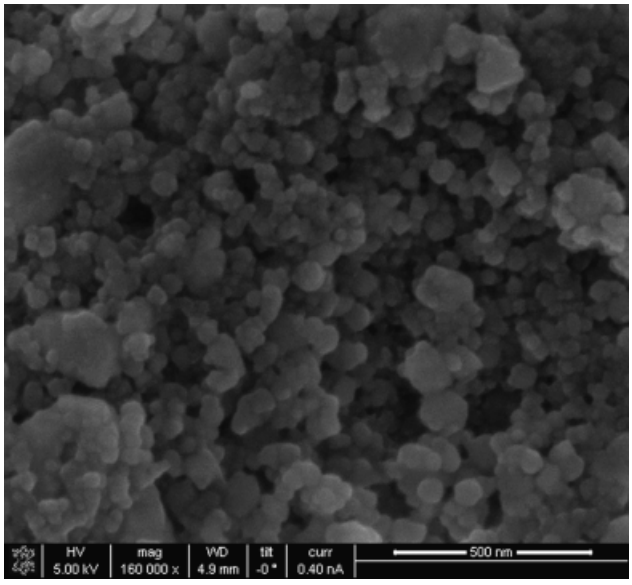

Fig. 7. High-resolution scanning electron microscopy of pellet from a 50:50 (mol:mol) mixture of liquid-feed flame spray pyrolysis *t*-ZrO_2 with δ-Al_2O_3 nanopowders heated at 10°C/min/air to 1120°C/6 h dwell. Scale bar is 500 nm.

densities <96% and micrometer-sized grains.[11–16] In contrast, our fully dense ZTA composites with 60 wt% (54 mol%, 42 vol%) *t*-ZrO_2 with grains <200 nm can be expected to offer much improved fractured toughness by the increase in ZrO_2 volume fraction (up to 42 vol%) for potential structural applications.

Several closing comments provide an important perspective to the above data. One might argue that because the proportion of *t*-ZrO_2 used in the current studies is greater than in the cited studies, the higher densification rates at lower temperatures observed might be expected given the work of Rhodes.[49] However, Magnani and Brillante describe sintering studies on both 60 wt% α-Al_2O_3:40 wt% 3YPSZ and 50 wt% α-Al_2O_3:50 wt% 2YPSZ wherein it was observed that these samples required heating at 1450° for 1 h to achieve 99.2%–99.8% densities. Samples from the same study were also HIPped yielding somewhat higher densities. HIPped samples showed slightly greater hardness but lower toughness because of partial transformation to the monoclinic phase. Also important is that samples with only 2 wt% yttria yielded higher toughnesses (8 vs 6 MPa · $m^{0.5}$) than those with 3 wt% and retained 100% tetragonality under the same processing conditions. Final AGSs were 200–300 nm whereas HIPped samples were 50% larger. Thus, it appears that we can achieve similar densities, smaller grain sizes, and retain the tetragonal phase without added yttria at temperatures 300°C less than in this study.

Two further pertinent publications from Srdić *et al.*[51,52] describe flame synthesis of very fine, 5 nm APS ZrO_2 powders doped with 3, 5, 15, or 30 mol% Al_2O_3. The authors report that the surface-doped 3 mol% material is 20% monoclinic with the remainder being either the cubic or tetragonal phase. These authors prepared compacts of the various powders and sintered them at temperatures up to 1100°C. They found that the pure zirconia powders were sintering to full density at 1000°C, which was 100°C below that found by Rhodes.[49] However, they found that the presence of even 3 mol% Al_2O_3 coatings made it much more difficult to sinter to full density and at 15 and 30 mol% Al_2O_3, they were unable to sinter to full density even at 1100°C with the same grain sizes. They argue that the presence of Al_2O_3 surface coatings significantly reduces sintering rates. Given that their materials had AGSs closer to 5 nm rather than the 30–50 nm found in this study would suggest that they should observe sintering to full density at these temperatures. They suggest that a solid solution forms between the alumina and zirconia at these particle sizes inhibiting densification. It is important to point out

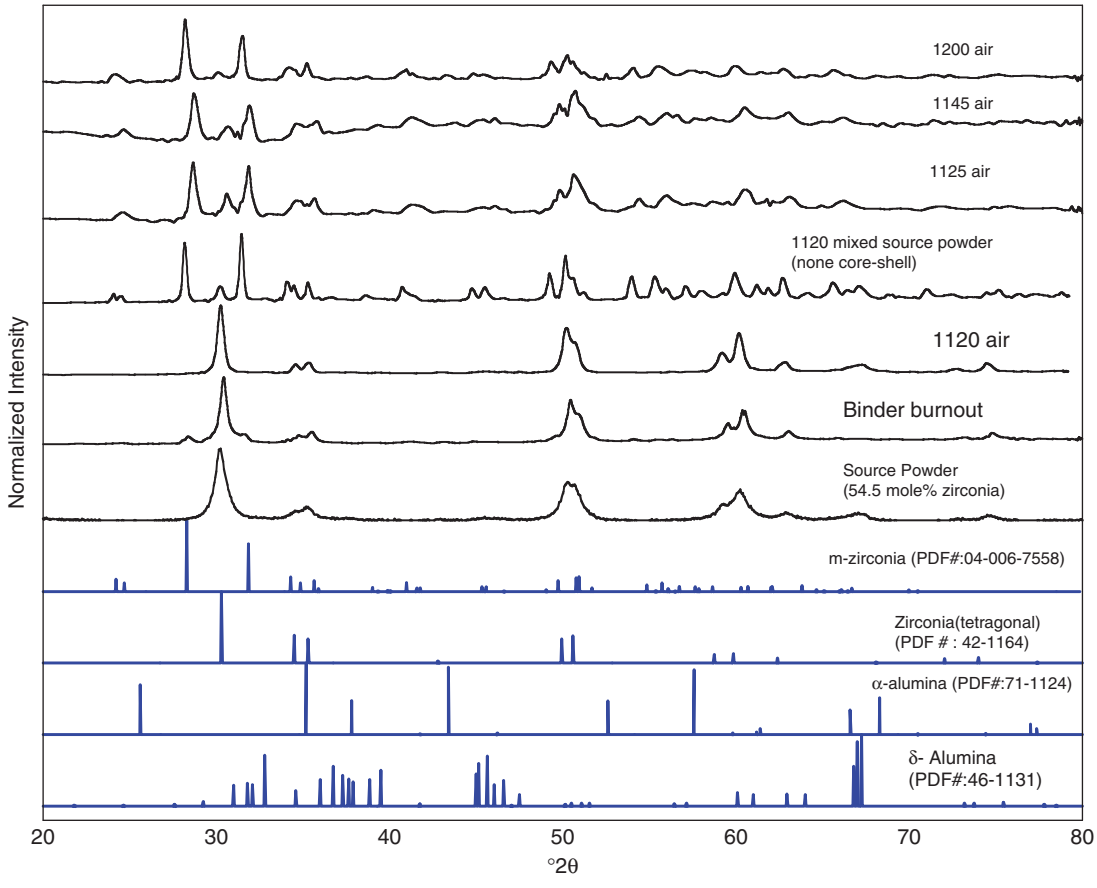

Fig. 8. X-ray diffractions of $(ZrO_2)_{0.54}(Al_2O_3)_{0.46}$ powders, and pellets heated to selected temperatures.

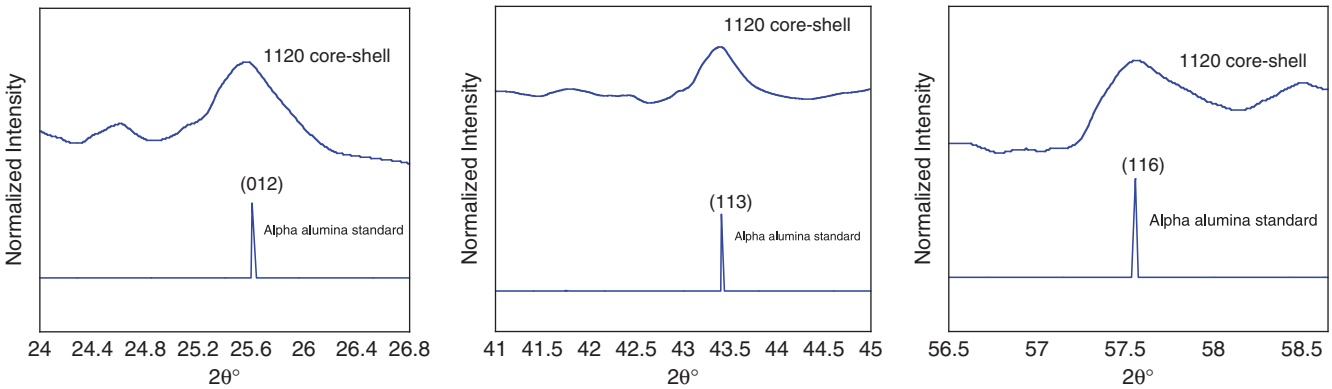

Fig. 9. Spot-by-spot X-ray diffractions of a $(ZrO_2)_{0.54}(Al_2O_3)_{0.46}$ pellet heated to 1120°C/6 h dwell.

that they did not describe the Al_2O_3 phase formed although it seems likely that it would be the same as what we see. Given that we see essentially complete densification at 1120°C with larger APS, we again suggest that the LF-FSP-derived materials are quite unique allowing the following conclusions.

IV. Conclusions

In this study, we demonstrated that it is possible to pressureless sinter $(t\text{-}ZrO_2)_{0.54}(\delta\text{-}Al_2O_3)_{0.46}$ core–shell nanostructured nanopowders to produce fully dense ZTA nanocomposites with $\geq 99\%$ densities and final grain sizes <200 nm at ≈ 1120°C. We were further demonstrated full densification while retaining the tetragonal phase without the need for yttria stabilization at $t\text{-}ZrO_2$ contents of 54 mol% (60 wt%) at much lower temperatures than used previously.[18] We also observe the transformation of the shell $\delta\text{-}Al_2O_3$ to $\alpha\text{-}Al_2O_3$ at temperatures below the normal phase transformation temperature of ≈ 1200°C. Finally, simple hand grinding demonstrates that these materials will offer the expected transformation toughening.

These results suggest an entirely new mechanism for processing ceramic composite materials through the use of core–shell powders wherein the shell consists of a ceramic (or glass) phase with a much higher rate of self-diffusion. At a minimum, this approach offers the potential to obtain a wide range of fully dense ZTA composites without HIPping and using much milder processing conditions than normally required for much lower $t\text{-}ZrO_2$ content ZTAs.

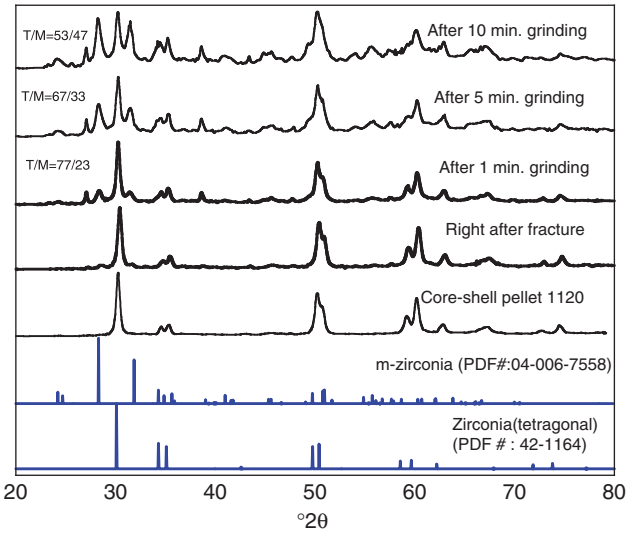

Fig. 10. X-ray diffraction patterns of pellets heated to 1120°C and following hand grinding as a function of time. T/M = wt% tetragonal phase in zirconia/wt% tetragonal phase in zirconia.

The potential to extend this approach to a variety of other materials exists. Thus, we expect our fully dense nanostructured ZTA composites to offer superior strength and fracture toughness (as suggested by the work of Magnani and Brillante[18]), thermal shock resistance, and thus potential for structural and especially biomedical applications. Overall, the resulting ultrafine and nanocomposites from the above materials but especially ZTA are expected to provide both greatly improved mechanical properties for diverse applications.[1–41]

References

[1]M. N. Rahaman, A. Yao, B. Sonny Bal, J. P. Garino, and M. D. Ries, "Ceramics for Prosthetic Hip and Knee Joint Replacement," *J. Am. Ceram. Soc.*, **90** [7] 1965–88 (2007).
[2]M. A. Meyers, A. Mishra, and D. J. Benson, "Mechanical Properties of Nanocrystalline Materials," *Pro. Mater. Sci.*, **51** [4] 427–556 (2006).
[3]M. J. Stiger, N. M. Yanar, M. G. Topping, F. S. Pettit, and G. H. Meier, "Thermal Barrier Coatings for the 21st Century," *Zeitschr. Metall.*, **90** [12] 1069–78 (1999).
[4]M. E. Roy, L. A. Whiteside, B. J. Katerberg, and J. A. Steiger, "Phase Transformation, Roughness, and Microhardness of Artificially Aged Yttria- and Magnesia-Stabilized Zirconia Femoral Heads," *J. Biomed. Mater. Res. Part A*, **83A** [4] 1096–102 (2006).
[5]T. G. Nieh and J. Wadsworth, "Superplastic Behavior of a Fine-Grained, Yttria-Stabilized, Tetragonal Zirconia Polycrystal (Y-TZP)," *Acta Metall. Mater.*, **38** [6] 1121–33 (1990).
[6]G. Stapper, M. Bernasconi, N. Nicoloso, and M. Parrinello, "Ab Initio Study of Structural and Electronic Properties of Yttria-Stabilized Cubic Zirconia," *Phys. Rev. B*, **59** [2] 797–810 (1999).
[7]C. P. Wang, K. B. Do, M. R. Beasley, T. H. Geballe, and R. H. Hammond, "Deposition of In-Plane Textured MgO on Amorphous Si_3N_4 Substrates by Ion-Beam-Assisted Deposition and Comparisons with Ion-Beam-Assisted Deposited Yttria-Stabilized-Zirconia," *Appl. Phys. Lett.*, **71** [20] 2955–7 (1997).
[8]S. D. Souza, S. J. Visco, and L. C. De Jonghe, "Reduced-Temperature Solid Oxide Fuel Cell Based on YSZ Thin-Film Electrolyte," *J. Electrochem. Soc.*, **144** [3] L35–7 (1997).
[9]R. M. Ormerod, "Solid Oxide Fuel Cell," *Chem. Soc. Rev.*, **32**, 17–28 (2003).
[10]K. Otsuka, S. Yokoyama, and A. Morikawa, "Catalytic Activity-Control and Selectivity-Control for Oxidative Coupling of Methane by Oxygen-Pumping Through Yttria-Stabilized Zirconia," *Chem. Lett.*, **3**, 319–22 (1985).
[11]A. J. Feighery and J. T. S. Irvine, "Effect of Alumina Additions Upon Electrical Properties of 8 mol.% Yttria-Stabilised Zirconia," *Solid State Ionics*, **121**, 209–16 (1999).
[12]J. Freim and J. Mckittrick, "Modeling and Fabrication of Fine-Grain Alumina–Zirconia Composites Produced from Nanocrystalline Precursors," *J. Am. Ceram. Soc.*, **81** [7] 1773–80 (1998).
[13]F. F. Lange, "Transformation Toughened ZrO_2: Correlations Between Grain Size Control and Composition in the System ZrO_2–Y_2O_3," *J. Am. Ceram. Soc.*, **69** [3] 240–2 (1986).
[14]R. J. Hannick, P. M. Kelly, and B. C. Muddle, "Transformation Toughening in Zirconia-Containing Ceramics," *J. Am. Ceram. Soc.*, **83** [3] 461–87 (2000).
[15]A. Suresh, M. J. Mayo, W. D. Porter, and C. J. Rawn, "Crystallite and Grain-Size-Dependent Phase Transformations in Yttria-Doped Zirconia," *J. Am. Ceram. Soc.*, **86** [2] 360–2 (2003).
[16]A. Bravo-Leon, Y. Morikawa, M. Kawahara, and M. J. Mayo, "Fracture Toughness of Nanocrystalline Tetragonal Zirconia with Low Yttria Content," *Acta Mater.*, **50**, 4555–62 (2002).
[17]R. A. Kimel and J. H. Adair, "Aqueous Synthesis at 200°C of Sub-10 Nanometer Yttria Tetragonally Stabilized Zirconia Using a Metal-Ligand Approach," *J. Am. Ceram. Soc.*, **88** [5] 1133–8 (2005).
[18]G. Magnani and A. Brillante, "Effect of the Composition and Sintering Process on Mechanical Properties and Residual Stresses in Zirconia–Alumina Composites," *J. Eur. Ceram. Soc.*, **25**, 3383–92 (2005).

[19]A. J. Feighery and J. T. S. Irvine, "Effect of Alumina Additions Upon Electrical Properties of 8 mol.% Yttria-Stabilised Zirconia," *Solid State Ionics*, **121**, 209–16 (1999).
[20]X. Guo, "Property Degradation of Tetragonal Zirconia Induced by Low-temperature Defect Reaction with Water Molecules," *Chem. Mater.*, **16** [21] 3988–94 (2004).
[21]I. Yamashita, K. Tsukuma, T. Tojo, H. Kawaji, and T. Atake, "Synchrotron X-Ray Study of the Crystal Structure and Hydrothermal Degradation of Yttria-Stabilized Tetragonal Zirconia Polycrystal," *J. Am. Ceram. Soc.*, **91** [5] 1634–9 (2008).
[22]R. J. Hannick, P. M. Kelly, and B. C. Muddle, "Transformation Toughening in Zirconia-Containing Ceramics," *J. Am. Ceram. Soc.*, **83** [3] 461–87 (2000).
[23]J. L. Wang and R. Stevens, "Zirconia-Toughened Alumina (ZTA) Ceramics," *J. Mater. Sci.*, **24**, 3421–40 (1989).
[24]N. Ramachandran and D. K. Shetty, "Rising Crack-Growth-Resistance (R-Curve) Behavior of Toughened Alumina and Silicon Nitride," *J. Am. Ceram. Soc.*, **74** [10] 2634–41 (1991).
[25]M. Guazzato, M. Albakry, S. P. Ringer, and M. V. Swain, "Strength, Fracture Toughness and Microstructure of a Selection of All-Ceramic Materials. Part II. Zirconia-Based Dental Ceramics," *Dental Mater.*, **20** [5] 449–56 (2004).
[26]P. F. Becher, K. B. Alexander, A. Bleier, S. B. Waters, and W. H. Warwick, "Influence of ZrO_2 Grain Size and Content on the Transformation Response in the Al_2O_3–ZrO_2 (12 mol% CeO_2) System," *J. Am. Ceram. Soc.*, **76** [3] 657–63 (1993).
[27]A. H. De Aza, J. Chevalier, G. Fantozzi, M. Schehl, and R. Torrecillas, "Crack Growth Resistance of Alumina, Zirconia and Zirconia Toughened Alumina Ceramics for Joint Prostheses," *Biomaterials*, **23** [3] 937–42 (2002).
[28]C. He, Y. S. Wang, J. S. Wallace, and S. M. Hsu, "Effect of Microstructure on the Wear Transition of Zirconia-Toughened Alumina," *Wear*, **162–164** [1] 314–21 (1993).
[29]X. He, Y. Z. Zhang, J. P. Mansell, and B. Su, "Zirconia Toughened Alumina Ceramic Foams for Potential Bone Graft Applications: Fabrication, Bioactivation, and Cellular Responses," *J. Mater. Sci.: Mater. Med.*, **19**, 2743–9 (2008).
[30]P. Zhu, Z. Lin, G. Chen, and I. Kiyohiko, "The Predictions and Applications of Fatigue Lifetime in Alumina and Zirconia Ceramics," *Int. J. Fat.*, **26** [10] 1109–14 (2004).
[31]A. Dakskobler and T. Kosmac, "The Preparation and Properties of Al_2O_3–ZrO_2 Composites with Corrugated Microstructures," *J. Eur. Ceram. Soc.*, **24**, 3351–7 (2004).
[32]J. Zarate, H. Juarez, M. E. Contreras, and R. Perez, "Experimental Design and Results from the Preparation of Precursor Powders of ZrO_2(3%Y_2O_3)/(10-95)%Al_2O_3 Composites," *Powder Technol*, **159** [3] 135–41 (2005).
[33]S. T. Aruna and K. S. Rajam, "Mixture of Fuels Approach for the Solution Combustion Synthesis of Al_2O_3–ZrO_2 Nanocomposites," *Mater. Res. Bull.*, **39**, 157–67 (2004).
[34]S. Bhaduri, S . B. Bhaduri, and E. Zhou, "Auto Ignition Synthesis and Consolidation of Al_2O_3–ZrO_2 Nano/Nano Composite Powders," *J. Mater. Res.*, **13** [1] 156–65 (1998).
[35]A. Leriche, G. Moortgat, F. Cambier, P. Homerin, F. Thevenot, G. Orange, and G. Fantozzi, *J. Eur. Ceram. Soc.*, **9** [3] 169–76 (1992).
[36]S. M. Barinov, V. F. Ponomarev, V. Ya, Shevchenko, and D. Shawran, *J. Mater. Sci. Lett.*, **14** [12] 871–3 (1995).
[37]D. Casellas, M. M. Nagl, L. Llanes, and M. Anglada, "Fracture Toughness of Alumina and ZTA Ceramics," *J. Mater. Proc. Technol.*, **143–144**, 148–52 (2003).
[38]W. H. Tuan, R. Z. Chen, T. C. Wang, C. H. Cheng, and P. S. Kuo, "Mechanical Properties of Al_2O_3/ZrO_2 Composites," *J. Eur. Ceram. Soc.*, **22**, 2827–33 (2002).
[39]D. Jayaseelan, T. Nishikawa, H. Awaji, and F . D. Gnanam, "Pressureless Sintering of Sol–Gel Derived Alumina–Zirconia Composites," *Mater. Sci. Eng.*, **A256** [1–2] 265–70 (1998).
[40]H. Yoshida, S. Hashimoto, and T. Yamamoto, "Dopant Effect on Grain Boundary Diffusivity in Polycrystalline Alumina," *Acta Mater.*, **53** [2] 433–40 (2005).
[41]J. Gopaul, W. C. Maskell, and K. E. Pitt, "Planar Oxygen Sensor Part I: Effect of Crazing of a Zirconia Crack on an Alumina Substrate," *J. Appl. Electrochem.*, **29** [1] 93–100 (1999).
[42]A. H. Heuer, "Oxygen and Aluminum Diffusion in α-Al_2O_3: How Much Do We Really Understand?," *J. Eur. Ceram. Soc.*, **28** [7] 1495–507 (2008).
[43]T. Hinklin, B. Toury, C. Gervais, F. Babonneau, J. J. Gislason, R. W. Morton, and R. M. Laine, "Liquid-Feed Flame Spray Pyrolysis of Metalloorganic and Inorganic Alumina Sources in the Production of Nanoalumina Powders," *Chem. Mater.*, **16** [1] 21–30 (2004).
[44]S. Kim, J. J. Gislason, R. W. Morton, X. Q. Pan, H. P. Sun, and R. M. Laine, "Liquid-Feed Flame Spray Pyrolysis of Nanopowders in the Alumina–Titania System," *Chem. Mater.*, **16** [12] 2336–43 (2004).
[45]J. A. Azurdia, J. Marchal, P. Shea, H. Sun, X. Q. Pan, and R. M. Laine, "Liquid-Feed Flame Spray Pyrolysis as a Method of Producing Mixed-Metal Oxide Nanopowders of Potential Interest as Catalytic Materials. Nanopowders Along the NiO–Al_2O_3 Tie Line Including $(NiO)_{0.22}(Al_2O_3)_{0.78}$, a New Inverse Spinel Composition," *Chem. Mater.*, **18** [3] 731–9 (2006).
[46]J. A. Azurdia, J. Marchal, and R. M. Laine, "Synthesis and Characterization of Mixed-Metal Oxide Nanopowders Along the CoO_x–Al_2O_3 Tie Line Using Liquid-Feed Flame Spray Pyrolysis," *J. Am. Ceram. Soc.*, **89** [9] 2749–56 (2006).
[47]M. Kim, T. R. Hinklin, and R. M. Laine, "Core–Shell Nanostructure Nanopowders Along $(CeO_x)_x(Al_2O_3)_{1-x}$ Tie-Line by Liquid-Feed Flame Spray Pyrolysis (LF-FSP)," *Chem. Mater.*, **20** [16] 5154–62 (2008).
[48]M. Kim, R. M. Laine, "Liquid-Feed Flame Spray Pyrolysis (LF-FSP) for Combinatorial Processing of Nanooxide Powders Along the $(ZrO_2)_{1-x}(Al_2O_3)_x$ Tie-Line. Phase Segregation and the Formation of Core–Shell Nanoparticles," *J. Ceram. Proc. Res.*, **8** [2] 129–36 (2007).
[49]W. H. Rhodes, "Agglomerate and Particle Size Effects on Sintering Yttria-Stabilized Zirconia," *J. Am. Ceram. Soc.*, **64** [1] 19–22 (1981).
[50]R. M. Laine, J. C. Marchal, H. P. Sun, and X. Q. Pan, "Nano-α-Al_2O_3 by Liquid-Feed Flame Spray Pyrolysis (LF-FSP) of Nano-Transition Aluminas," *Nat. Mater.*, **5** [9] 710–2 (2006).
[51]V. V. Srdić, M. Winterer, A. Möller, G. Miehe, and H. Hahn, "Nanocrystalline Zirconia Surface Doped with Alumina: Chemical Vapor Synthesis, Characterization, and Properties," *J. Am. Ceram. Soc.*, **84** [12] 2771–6 (2001).
[52]V. V. Srdić, M. Winterer, and H. Hahn, "Sintering Behavior of Nanocrystalline Zirconia Doped with Alumina Prepared by Chemical Vapor Synthesis," *J. Am. Ceram. Soc.*, **83** [8] 1853–60 (2000). □